Penetration Pathways Induced by Low-Frequency Sonophoresis with Physical and Chemical Enhancers: Iron Oxide Nanoparticles versus Lanthanum Nitrates

Sang Eun Lee[1,5], Ki Ju Choi[2,5], Gopinathan K. Menon[3], Hyun Jung Kim[1], Eung Ho Choi[4], Sung Ku Ahn[4] and Seung Hun Lee[1]

Low-frequency sonophoresis (LFS) has been shown to disrupt the structure of stratum corneum (SC) lipid bilayers and enhance SC permeability. In this study, we examined the penetration pathway of lanthanum nitrate ($LaNO_3$) tracer in viable epidermis after combined treatment of LFS and tape stripping (TS), as a physical enhancer, or oleic acid (OA) application, as a chemical enhancer, using transmission electron microscopy (TEM). As a positive control, we visualized the passive diffusion pathway of $LaNO_3$ and iron oxide (Fe_3O_4) nanoparticles after the incision of hairless mouse skin. Next, we applied LFS immediately after TS or OA application and visualized the penetration pathway of $LaNO_3$. Each treatment showed restricted penetration to the SC–stratum granulosum (SG) interface or upper SG layer. However, the additional application of LFS induced diffuse intracellular distribution of $LaNO_3$ throughout the viable epidermis. Quantitative analysis also revealed that combined treatment significantly increases $LaNO_3$ penetration into viable epidermis when compared with each treatment. Our ultrastructural findings show the synergistic effect of LFS and TS or OA application on transdermal drug delivery. We also found that this combined treatment enhances the penetration of $LaNO_3$ through the viable epidermis through an intracellular pathway.

Journal of Investigative Dermatology (2010) **130,** 1063–1072; doi:10.1038/jid.2009.361; published online 26 November 2009

INTRODUCTION

Low-frequency sonophoresis (LFS) is a method of enhancing skin permeability to drugs using ultrasound at a low frequency (20–100 kHz). LFS has been shown to enhance transdermal transport of a variety of molecules, including insulin (Kost *et al.*, 2000), morphine (Monti *et al.*, 2001), glucose (Merino *et al.*, 2003), lidocaine (Becker *et al.*, 2005), heparin, and tetanus toxoid vaccine (Ogura *et al.*, 2008). As stratum corneum (SC) is the most significant barrier to transdermal delivery (Elias, 1983), many ultrastructural studies have focused on analyzing the permeation pathways through the SC during LFS, using various visualization methods. It is now accepted that lacunae spaces that are present in normal lipid bilayers of SC and LFS increase the spatial frequency of lacunae, which possibly leads to the formation of a well-connected three-dimensional porous network in the SC (Paliwal *et al.*, 2006). These dilated lacuna spaces during LFS are considered the putative pathway for permeation of polar and nonpolar molecules across the SC (Menon and Elias, 1997; Tezel *et al.*, 2002, 2003). Recently, these ultrastructural modifications of the SC during LFS have been illustrated using quantum dots as tracer nanoparticles (Paliwal *et al.*, 2006).

Recently, therapeutic applications of ultrasound-mediated transdermal drug transport have been extended to various areas, including chemotherapy, tissue engineering, and gene therapy (Ogura *et al.*, 2008). For therapeutic efficacy, a deep penetration of drugs not only into the SC layers but also into the viable epidermis and capillary plexus may be important. However, although many studies have been performed to identify the LFS-induced penetration pathways within the SC (Menon and Elias, 1997; Paliwal *et al.*, 2006), the LFS-induced penetration pathways in the viable epidermis are largely unanalyzed. For these reasons, in this analysis, we primarily focused on the penetration pathway of tracers in the viable skin layers. Previous studies have shown that the effects of sonophoresis act synergistically with various other physicochemical enhancement methods on transdermal drug transport (Mitragotri and Kost, 2004). Among the chemical enhancers, oleic acid (OA) has been suggested to act by

[1]*Department of Dermatology and Cutaneous Biology Research Institute, Yonsei University College of Medicine, Seoul, Korea;* [2]*Department of Oriental Medicinal Materials and Processing, Kyung Hee University College of Life Science, Yongin, Korea;* [3]*International Specialty Products, Yonsei University Wonju College of Medicine, Wonju, Korea and* [4]*Department of Dermatology, Yonsei University Wonju College of Medicine, Wonju, Korea*

[5]*These two authors contributed equally to this work*

Correspondence: Seung Hun Lee, Department of Dermatology, Gangnam Severance Hospital, Yonsei University College of Medicine, 712 Eonjuro, Kangnam-gu, Seoul 135-720, Korea. E-mail: ydshderm@yuhs.ac

Abbreviations: LFS, low-frequency sonophoresis; OA, oleic acid; SC, stratum corneum; SG, stratum granulosum; TEM, transmission electron microscopy

Received 2 April 2009; revised 24 September 2009; accepted 28 September 2009; published online 26 November 2009

extracting a fraction of the endogenous SC membrane components, and by promoting phase separation within SC lipids, thereby decreasing the barrier permeability function (Naik *et al.*, 1995). Tape stripping (TS) may enhance penetration by physically reducing SC thickness and facilitating the delivery of tracers percutaneously. From these results, we hypothesized that LFS with chemical or physical enhancer could be used to deliver the tracers deep into the viable epidermis allowing us to analyze the penetration pathway of tracers in the viable skin layers. On the basis of these assumptions, OA application and TS were performed in combination with LFS as a chemical and physical enhancer, respectively. Then, we analyzed and visualized the effects of these combination treatments on the permeation of an electron-dense tracer, lanthanum nitrate ($LaNO_3$), through the viable epidermis using transmission electron microscopy (TEM). As the aim of this study was to elucidate the penetration pathway of tracers across the viable epidermis after these combined treatments, it was necessary to perform the passive diffusion experiments with an incision technique for delivering tracers across an SC barrier as a positive control. Recently, nano-sized particles, whose dimensions are <100 nm, have received significant attention for biomedical and cosmetic applications; however, toxicological issues, including the probability of penetration into skin and the possible intrinsic toxicity, remain major concerns (Jin and Ye, 2007; Nohynek *et al.*, 2008; Baroli, 2009). Moreover, a recent study, using light transmission microscope and TEM (Baroli *et al.*, 2007), showed that metallic nanoparticles (maghemite and iron nanoparticles), smaller than 10 nm, were able to passively penetrate into human full-thickness skin through the SC lipidic matrix and aggregated SC-viable epidermis junction, occasionally reaching the viable epidermis. For these reasons, we also analyzed the passive diffusion pathway of iron oxide (Fe_3O_4) nanoparticles across the viable epidermis and compared it with the pathway of $LaNO_3$.

RESULTS

Nanoparticle characterization

TEM visualization revealed that Fe_3O_4 nanoparticles were uniform in size and as small as 4.7–10.6 nm (average 8.67 ± 2.8 nm in Figure 1). Fe_3O_4 nanoparticles were found as electron-dense individual particles and had a uniform cubic shape. In the absence of any surface modification, iron oxide nanoparticles in this study have no surface charge.

Ultrastructural changes of stratum corneum after low-frequency sonophoresis (LFS)

We observed the ultrastructural changes on the surface of SC after treatment with low-frequency ultrasound using scanning electron microscopy and TEM. Approximately 1- to 2-μm-sized pores were observed on the surface of corneocytes after 5 minutes of LFS in the scanning electron microscopy images (arrow heads, Figure 2b). A TEM study to assess the penetration of $LaNO_3$ in the SC showed that in the absence of ultrasound, $LaNO_3$ was found to be restricted to the top layers of SC (Figure 2c). After the application of ultrasound, $LaNO_3$ was distributed inside the corneocytes of the uppermost two layers of SC in the TEM images (Figure 2d). To assess the LFS-induced ultrastructural changes in the lipid lamellae, we next examined the LFS-treated epidermis using ruthenium tetroxide postfixation. In the tightly packed lipid bilayers of the SC, discrete elongated defects (dilated lacunae) were found after LFS (arrow, Figure 2e). Occasionally, rolled-up lipids were found in the dilated lacunae (arrow, Figure 2f).

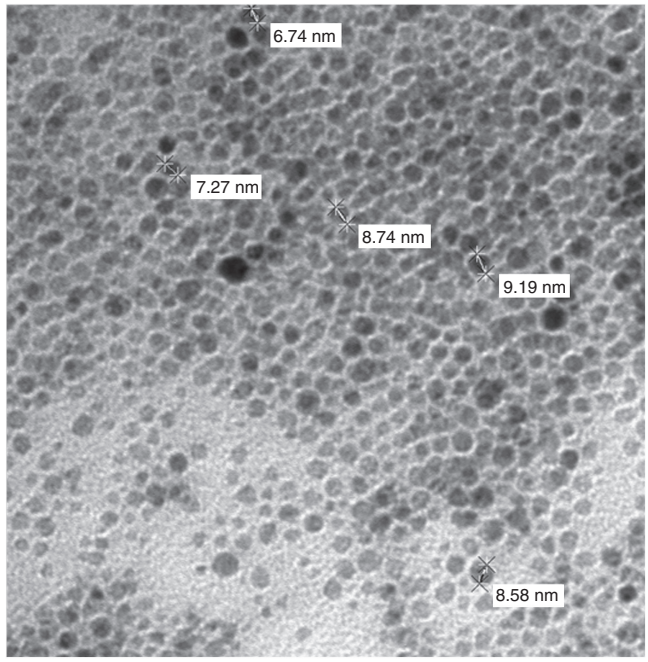

Figure 1. TEM micrograph of iron oxide nanoparticles.

Different diffusion pathway of $LaNO_3$ and Fe_3O_4 nanoparticle in the viable epidermis

To identify and visualize the passive diffusion pathway within the underlying nucleated layers of epidermis, we made a superficial incision over the back of the mouse and then applied $LaNO_3$ or Fe_3O_4. TEM images revealed a longitudinal fissure formed by an incision extended to the SG which measured approximately 1 μm in width. $LaNO_3$ was found to spread from the fissure into the adjacent keratinocytes (Figure 3a). The $LaNO_3$, which was immediately adjacent to the incision site, showed diffuse intracellular distribution and was also detected in the intercellular spaces (Figure 3b). In contrast to the area near the injury, in the area 30 μm distant from the incision site, $LaNO_3$ was observed primarily in the intercellular spaces (arrow, Figure 3c). In the area adjacent from the injury, both $LaNO_3$ and Fe_3O_4 showed a similar pattern of distribution. As shown in the uppermost SC, both tracers were found in the cytoplasm of corneocytes and in the intercellular lipid lamellae (Figures 4a and 5a). However, in the area 30 μm distant from the incision, the penetration pattern of the two kinds of tracers differed. As shown in the

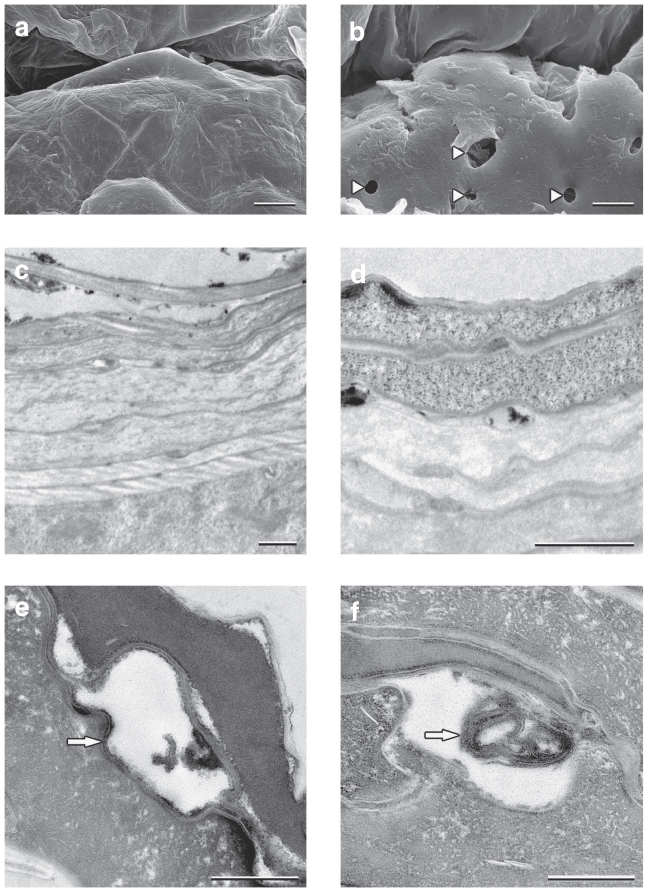

Figure 2. The ultrastructural changes on the SC surface and the penetration pathways of lanthanum nitrates after treatment with LFS, and TEM images of SC after treatment with LFS using ruthenium tetroxide fixation. (**a**) After 5 minutes of treatment with LFS, 1- to 2-μm-sized pores (**b**, arrowheads) were observed on the SC surfaces, which were not observed on the normal SC surface. (**b**) The scanning electron microscopy findings on the SC surface of mouse skin treated with LFS. (**c**) TEM findings in the SC after application of $LaNO_3$. In the absence of LFS, $LaNO_3$ was found to be restricted to the intercellular spaces of the upper SC. (**d**) In contrast, after 5 minutes of treatment with LFS, $LaNO_3$ was found in the intercellular and intracellular domains of the corneocytes in the upper SC. (**e**, arrow) After 5 minutes of treatment of LFS, 2- to 4-μm expansions in lacunae were observed in the widened intercellular spaces of the SC. (**f**, arrow) In some sections, rolled-up lipids were also observed in the dilated lacunae. Scale bar = 2 μm.

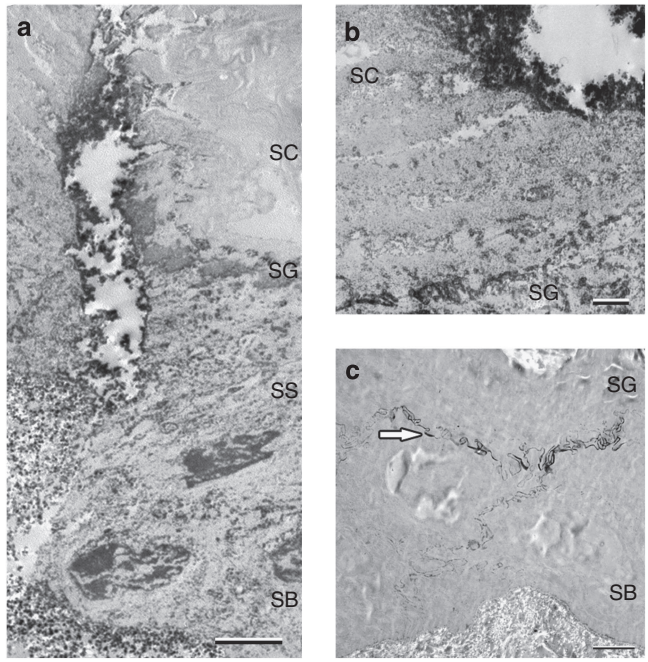

Figure 3. Transmission electron micrographs of mouse skin sections after application of $LaNO_3$ after cutting a vertical incision. (**a**) After cutting the back skin of the mouse with a sharp blade, we applied $LaNO_3$ and observed the passive diffusion pathways of $LaNO_3$ with TEM. A longitudinal fissure formed by incision extended to the stratum spinosum and measured about 1 μm in width. $LaNO_3$ was found to spread from the fissure into the adjacent tissue. (**b**) Enlarged view of the region near the incision site. $LaNO_3$ immediately adjacent to the incision site showed diffuse cytoplasmic distribution and is also detected in the intracellular spaces. (**c**, arrow) In contrast with the region near the incision site, at 30 μm distance from the incision site, $LaNO_3$ was observed primarily in the intercellular spaces. Scale bar = 1 μm.

nucleated viable epidermis, $LaNO_3$ was observed to be localized in the intercellular spaces (Figure 4b). In contrast, Fe_3O_4 nanoparticles were observed to be diffusely distributed in the intracellular spaces (Figure 5b).

Permeation pathways of $LaNO_3$ after LFS combined with other penetration enhancement methods

To penetrate $LaNO_3$ deeply into the viable epidermis and assess the permeation pathway in the viable epidermis, we used two different penetration enhancement methods, including chemical enhancer and TS before the application of ultrasound. $LaNO_3$ applied to tape-stripped skin was observed to permeate across the SC into the SC–SG interface and occasionally into the upper SG layer (Figure 6a–c). This observation represents a defective barrier function because of the removal of SC components by TS. We found that in the uppermost SC, $LaNO_3$ was presented inside the corneocytes, whereas in the underlying layers of lower SC and upper SG, $LaNO_3$ was localized in the intercellular domains (Figure 6b and c). However, when the tape-stripped skin was exposed to ultrasound in the presence of $LaNO_3$, the tracers were observed to be uniformly distributed throughout the epidermis. $LaNO_3$ penetrated into the intracellular and intercellular spaces extending to the stratum basalis layer of the viable epidermis (Figure 6d–f). Next, we used a chemical enhancer. The effects of OA-induced skin penetration enhancement have been previously reported using the lanthanum perfusion method. Consistent with the previous report, we observed that $LaNO_3$ extended into the intercellular spaces of the SC and into the SC–SG interface in OA-treated epidermis (Figure 7a). In the uppermost SC, the tracers penetrated inside the corneocytes in OA-treated epidermis in a manner similar to that observed in tape-stripped skin (Figure 7b). When the OA-treated skin was exposed to ultrasound in the presence of $LaNO_3$, the tracers were observed to be uniformly distributed in the intracellular and intercellular domains throughout the

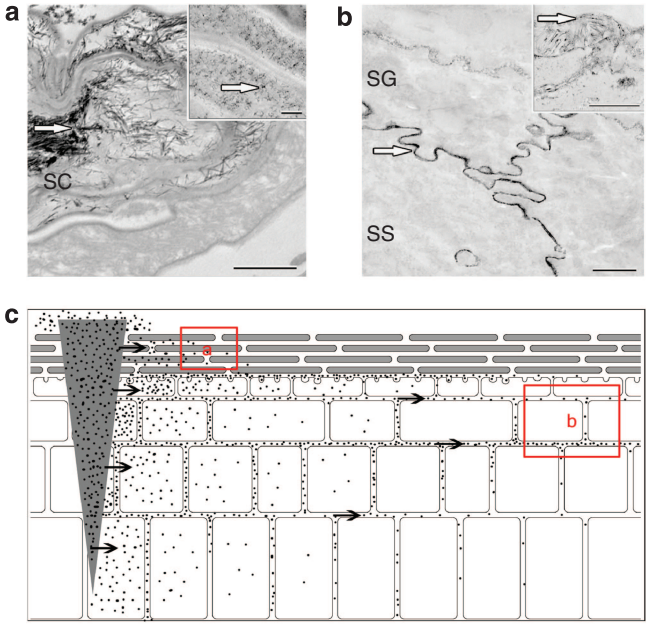

Figure 4. Transmission electron micrographs of mouse skin sections after application of $LaNO_3$ after making an incision and diagram of a passive diffusion pathway of $LaNO_3$. After cutting the skin with a sharp blade, we applied $LaNO_3$ and visualized the distribution of tracers immediately adjacent to the incision site and at 30 μm distance from the incision site with TEM. (**a**) In the SC, near the incision sites, $LaNO_3$ was observed in the intracellular domains of corneocytes (**a**, arrows) (inset shows the enlarged view of corneocytes). (**b**) In contrast, at 30 μm distance from the incision site, $LaNO_3$ was observed primarily in the intercellular spaces (**b**, arrows) (inset shows the enlarged view of SC–SG interface). (**c**) Diagram shows the passive diffusion pathway of $LaNO_3$. Scale bar = 0.5 μm.

epidermis, similar to the distribution seen in TS/LFS-treated skin (Figure 7d–f).

Quantitative analysis of the penetration of $LaNO_3$

The number density and area density of the electron-dense dots of $LaNO_3$, which penetrated into the SC, significantly increased in LFS-treated skin, tape-stripped skin, OA-treated skin, TS/LFS-treated skin, and OA/LFS-treated skin compared to those of controls ($P<0.005$) (Figure 8a and b). The number density of $LaNO_3$, which penetrated into the viable epidermis from the SB to SG layers, was about 6.34-fold and 28.13-fold higher in OA/LFS-treated skin compared with that of OA-treated skin ($P=0.0025$) and LFS-treated skin ($P=0.0038$), respectively. The number density of $LaNO_3$, which penetrated into the viable epidermis, was about 4.04- and 41.88-fold higher in TS/LFS-treated skin compared with that of the tape-stripped skin ($P=0.0047$) and LFS-treated skin ($P=0.0015$), respectively (Figure 8c). The area density of $LaNO_3$, which penetrated into the viable epidermis, was about 1.84- and 18.4-fold higher in OA/LFS-treated skin compared with that of the OA-treated skin ($P=0.0068$) and LFS-treated skin ($P=0.0019$), respectively. The area density of $LaNO_3$, which penetrated into the viable epidermis, was about 1.56- and 19-fold higher in TS/LFS-treated skin compared with that of the tape-stripped skin ($P=0.0053$) and LFS-treated skin ($P=0.0025$), respectively (Figure 8d). These results suggest that the combined treatment of LFS and OA application or TS synergistically enhance the delivery of tracers into the viable epidermis.

DISCUSSION

Consistent with previous observations, we found dilated lacuna spaces within the intercorneocyte lipid lamellae after LFS using TEM. The surface of SC after LFS application showed several 1- to 2-μm-sized pores in the scanning electron microscopy image. It has been shown that asymmetrical cavitation bubble collapse near the SC surface produces an acoustic microjet that might directly penetrate into the SC and disrupt the structure (Mitragotri and Kost, 2004). Initial damage in the membrane of the outmost cell layer by an acoustic microjet leads to the replacement of the original cell contents by nearby water and induces the formation of microbubbles in the second cell layer. Pores on the surface of SC, which are shown in Figure 2, can be thought of as the passing marks of a microjet. We also showed that LFS delivered $LaNO_3$ into the intracellular domain of corneocytes at the uppermost two layers of SC in the TEM images and that direct permeation at the upper SC might be because of asymmetric bubble collapse at the SC surface and rupture of the membrane of the next deeper cells.

In this study, we used three different techniques to enhance skin permeability, including LFS, TS as a physical enhancer, and OA application as a chemical enhancer. A single application of each technique showed limited penetration of $LaNO_3$, which penetrated the skin across the SC and reached and aggregated to the SC-SG junction and occasionally presented in the upper layers of SG, suggesting that in addition to the SC barrier, the junction between the SC and the viable epidermis is also an important barrier to skin penetration. The tight junctions in the granular layer, non-degraded corneodesmosomes, and more tightly compacted SC near the viable epidermis might form a structural barrier at the SC-viable epidermis junction (Kierszenbaum, 2002; Baroli *et al.*, 2007). In the passive diffusion experiments, which we used as a positive penetration control, we showed that both $LaNO_3$ and Fe_3O_4 nanoparticles permeated the viable epidermis by passive diffusion into the SB layer, after disruption of the SC barrier with a superficial incision. Our results also showed that in the area adjacent to the incision site, both $LaNO_3$ and Fe_3O_4 showed diffuse intracellular and intercellular distributions; however, in the area distant from the incision, $LaNO_3$ was observed primarily in the intercellular spaces. On the other hand, Fe_3O_4 was observed to be diffusely distributed in the intracellular spaces. This different pattern of diffusion through the viable epidermis between $LaNO_3$ and Fe_3O_4 could be explained by the different physicochemical characteristics of the two tracers. The dimension or particle size has been suggested as the most important property to influence nanoparticle permeation and diffusion through the skin (Baroli *et al.*, 2007; Rouse *et al.*, 2007). The dimensions of $LaNO_3$ and Fe_3O_4 nanoparticles were 2–10 and 4.6–10 nm, respectively, from the TEM measurement. Although the possibility and reversibility of

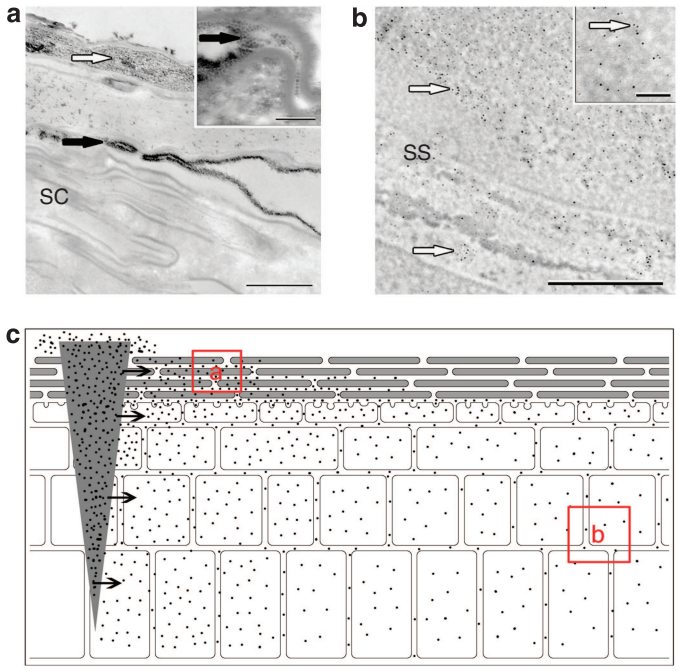

Figure 5. Transmission electron micrographs of mouse skin sections after application of Fe_3O_4 nanoparticles after making an incision and diagram of a passive diffusion pathway of Fe_3O_4. After cutting the skin with a sharp blade, we applied Fe_3O_4 and visualized the distribution of Fe_3O_4 immediately adjacent to the incision site and at 30 μm distance from the incision site with TEM. (**a**) In the SC, near the incision sites, Fe_3O_4 was observed in the intracellular domains of corneocytes (**a**, arrow) and within the intercellular lipid lamellae (**a**, closed arrow) (inset shows the enlarged view of intercellular lipid lamellae). (**b**) In contrast, at 30 μm distance from the incision site, Fe_3O_4 was observed to be uniformly distributed in the intracellular spaces (**b**, arrows) (inset shows the enlarged view of intracellular spaces). (**c**) Diagram shows the passive diffusion pathway of Fe_3O_4 nanoparticles. Scale bar = 0.5 μm.

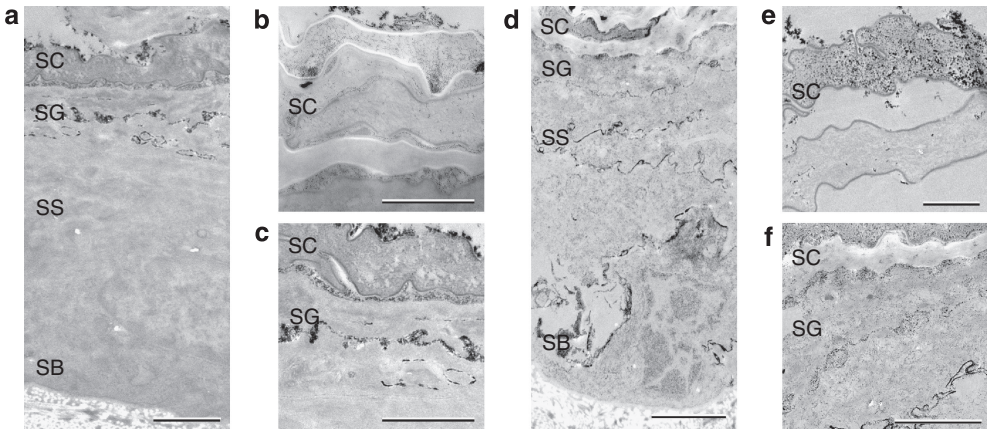

Figure 6. Transmission electron micrographs of mouse skin sections after tape stripping or LFS following tape stripping in the presence of $LaNO_3$. We applied $LaNO_3$ to tape-stripped mouse skin or skin treated with LFS after TS. (**a**) In the tape-stripped skin, TEM images show the $LaNO_3$ penetrating into the SC and upper SG. (**b**) In the enlarged view of the SC, $LaNO_3$ was present within the intracellular domains of corneocytes at the upper SC and also in the intercellular spaces. (**c**) In the enlarged view of the SC–SG interface, $LaNO_3$ was present at the SC–SG interface and intercellular spaces at the upper SG. (**d**) After TS/LFS treatment, $LaNO_3$ was observed to be diffusely distributed in the underlying epidermis, even in the SB layer. (**e**) In the enlarged view of the SC, $LaNO_3$ was present within the intracellular domains of corneocytes at the upper SC and also in the intercellular spaces. (**f**) In the enlarged view of the underlying epidermis, $LaNO_3$ was observed to be diffusely distributed in the intracellular and intercellular spaces. Scale bars = 2 μm (**a**, **d**), 1 μm (**b**, **c**, **e**, **f**).

aggregation of these particles *in vivo* cannot be ruled out, we could assume that both particles had similar dimensions. Along with their dimensions, the shape, superficial properties such as charges and polarity, and the stability of nanoparticles may further affect the penetration route and the depth of penetration across the skin (Baroli, 2009). As both tracer solutions were identical in concentration and contact time, one of the possible explanations for this difference in penetration route is surface charge. It was found that, owing to the charge of the lipid membrane, intermolecular forces

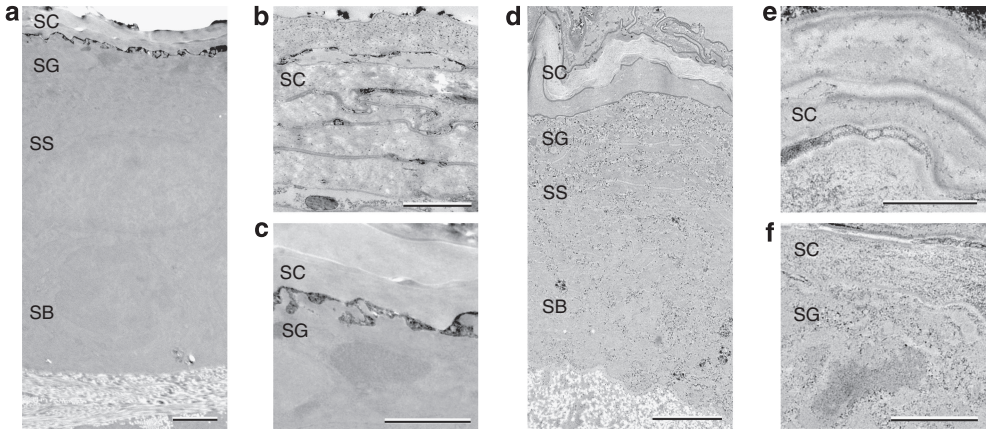

Figure 7. Transmission electron micrographs of mouse skin sections after OA application and LFS following OA application in the presence of $LaNO_3$. We applied $LaNO_3$ to OA-treated mouse skin or skin treated with LFS after OA application. (**a**) In the OA-treated skin, TEM images show the $LaNO_3$ penetrating into the SC and SC–SG interface. (**b**) In the enlarged view of the SC, $LaNO_3$ was present within the intracellular domains of corneocytes at the upper SC and also in the intercellular spaces. (**c**) In the enlarged view of the SC–SG interface, $LaNO_3$ was limited to the SC–SG interface. (**d**) After treatment with LFS following OA application, $LaNO_3$ was observed to be diffusely distributed in the underlying epidermis, even in the SB layer. (**e**) In the enlarged view of the SC, $LaNO_3$ was present within the intracellular domains of corneocytes at the upper SC and also in the intercellular spaces. (**f**) In the enlarged view of the underlying epidermis, $LaNO_3$ was observed to be diffusely distributed in the intracellular and intercellular spaces. Scale bars = 2 μm (**a**, **d**), 1 μm (**b**, **c**, **e**, **f**).

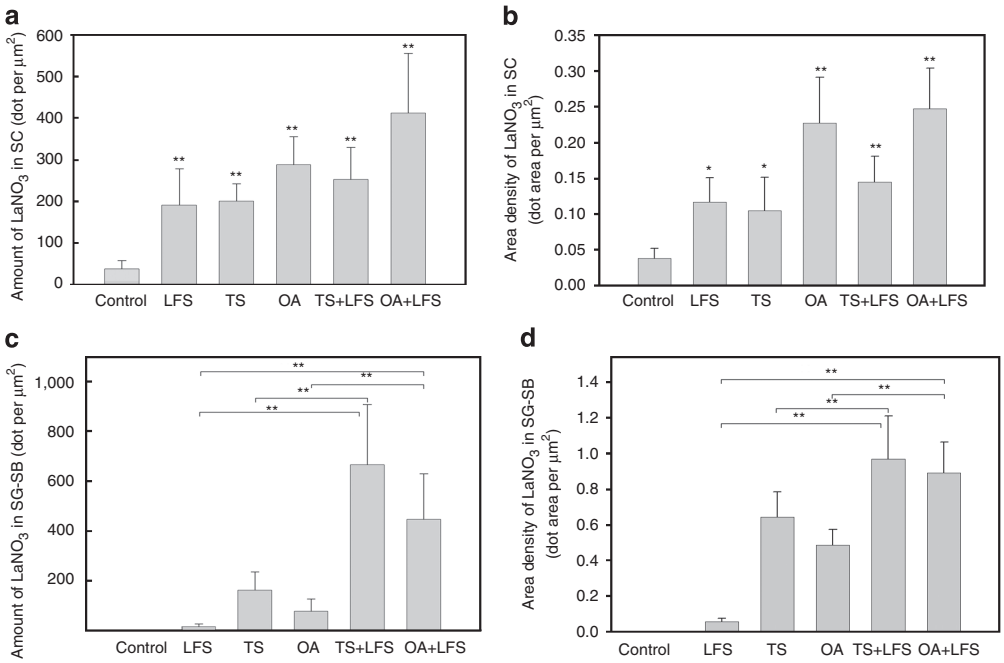

Figure 8. Quantitative analysis of the penetration of $LaNO_3$. (**a**) The number density and (**b**) area density of $LaNO_3$ penetrated into the SC increased in LFS-treated skin, tape-stripped skin, OA-applied skin, TS/LFS-treated skin, and OA/LFS-treated skin compared with controls ($P<0.005$). (**c**) The number density of $LaNO_3$ penetrated into the viable epidermis from the SB to the SG layer increased in TS/LFS-treated skin compared with that of the tape-stripped skin ($P=0.0047$) and LFS-treated skin ($P=0.0015$). OA/LFS-treated skin showed significantly increased number density of $LaNO_3$ penetrated into the viable epidermis compared with that of the OA-treated skin ($P=0.0025$) and LFS-treated skin ($P=0.0038$). (**d**) The area density of $LaNO_3$ penetrated into the viable epidermis increased in TS/LFS-treated skin compared with that of the tape-stripped skin ($P=0.0053$) and LFS-treated skin ($P=0.0025$). OA/LFS-treated skin showed significantly increased area density of $LaNO_3$ penetrated into the viable epidermis compared with that of the OA-treated skin ($P=0.0068$) and LFS-treated skin ($P=0.0019$) (**significant difference; $P<0.01$).

occurred between penetrants and cellular lipid bilayers during the penetration process and a high partial charge on the penetrant increased these intermolecular interactions and retarded penetration (Degim, 2005). For this reason, biological membranes are impermeable to most polar or charged molecules, but permeable to nonpolar compounds. Therefore, $LaNO_3$, the well-known ionic tracer, is expected to be unable to penetrate into the intercellular lipid bilayers

because of its surface charge, thereby spreading primarily in the intercellular spaces, whereas Fe_3O_4 nanoparticles with no surface modification, which did not present surface charge, could penetrate into the cell membrane and spread diffusely through the intracellular domains. Iron oxide nanoparticles have attracted interest because of their potential applications in biomedicine, including imaging, magnetic-induced target drug delivery, magnetic transfection of cells, tumor destruction by hyperthermia, photodynamic therapy, and biosensors for early detection of cancer, diabetes, and atherosclerosis (Penn *et al.*, 2003; Gupta and Gupta, 2005; Neuberger *et al.*, 2005; Wang *et al.*, 2007; Bechet *et al.*, 2008). With appropriate surface coatings, magnetic nanoparticles have also been used as cosmetic agents (Baroli, 2009). Our results suggest that if iron oxide nanoparticles <10 nm are accidentally in contact with the barrier-impaired skin or intentionally applied to diseased skin for therapeutic purposes, they could readily diffuse the viable epidermis through intracellular routes. However, care should be taken when generalizing our results using iron oxide nanoparticles without any surface modification to the clinically applied iron oxide-based multifunctional nanoparticles, because the surface property of the nanoparticle changes with functional ligands and the penetration mechanism of the nanoparticle is affected by these modified surface properties.

In our study, we found that TS or OA application pretreatment that was followed by LFS application enhanced the penetration depth of $LaNO_3$ into the SB layer compared with the penetration depth after each treatment of LFS, TS, or OA application, which showed limited penetration of $LaNO_3$ to the SC-viable epidermis junction or upper layer of the SG. These results are in agreement with previous studies showing the synergistic effects between LFS and various enhancers on transdermal drug transport and suggest that LFS combined with chemical or physical enhancers is as effective in enhancing skin permeability as direct skin injury, such as incision. Consistent with these electron microscopic observations, quantitative analysis of tracer penetration also revealed the synergistic effects of LFS with TS or OA application (Figure 8). Considering the possibility of $LaNO_3$ aggregation *in vivo*, we analyzed and quantified both the number density and area density of lanthanum nitrates in TEM images. LFS application on tape-stripped skin increased the number density of $LaNO_3$ penetrated into the viable epidermal layers by 41.88- and 4.04-fold, respectively, compared with the penetration after the application of either LFS or TS alone. The area density of $LaNO_3$ penetrated into the viable epidermis after TS/LFS treatment showed similar synergistic enhancement (19- and 1.56-fold increase, respectively, compared with the penetration following the application of either LFS or TS alone). The physical penetration enhancement methods, such as microscission, thermal poration, radiofrequency ablation, and microneedle application, have been shown to increase skin permeability to various therapeutic compounds by creating micron-scale pathways within the skin, thereby breaching the SC barrier temporarily (Prausnitz and Langer, 2008). TS could also reduce the physical barrier of the skin by reducing SC thickness and may facilitate the intraepidermal drug delivery. LFS has also been shown to target its effects on the SC barrier by disrupting lipid bilayers of SC, and therefore the combination treatment of TS and LFS could act synergistically on disrupting the SC barrier and enhancing the skin permeability. Our results also showed that the application of LFS in combination with OA synergistically enhances the number and area density of $LaNO_3$ penetrated into the viable epidermis compared with each treatment alone. OA pretreatment immediately followed by application of LFS increased the number density of $LaNO_3$ penetrated into the viable epidermis by 28.13- and 6.34-fold, respectively, compared with the penetration after the application of either LFS or OA application alone. The area density of $LaNO_3$ penetrated into the viable epidermis after OA/LFS treatment showed similar synergistic enhancement (18.4- and 1.84-fold increase, respectively, compared with the penetration after the application of either LFS or OA application alone). These results are in agreement with previous studies that have suggested that LFS acts synergistically with various chemical penetration enhancers. Mitragotri *et al.* (2000) reported that sodium lauryl sulfate enhanced skin permeability to mannitol synergistically in combination with ultrasound. Johnson *et al.* (1996) reported that the combined application of linoleic acid and ethanol with ultrasound increased corticosteroid flux by up to 13,000-fold compared with passive flux, which was higher than that induced by each treatment alone. El-Kamel *et al.* (2008) reported the synergistic effect of the chemical enhancers, 1% OA or 1% dodecylamine, and sonophoresis on testosterone transdermal delivery. The proposed mechanisms for these synergistic effects of ultrasound and chemical enhancers on transdermal drug transport are that the cavitation produced by ultrasound may induce mixing and facilitate the dispersion of the chemical enhancer with SC lipids (Johnson *et al.*, 1996; Mitragotri, 2000). OA has been used as a skin penetration enhancer through the mechanisms of lipid fluidization and lipid phase separation (Naik *et al.*, 1995). In addition, a recent ultrastructural study has shown that OA application resulted in the formation of expanded lacunae and distinct disorganization of the SC lipid structures *in vivo*, suggesting that OA may enhance skin permeability by dual mechanisms involving SC lipid bilayer perturbation and lacunae formation (Jiang and Zhou, 2003).

It is interesting that the penetration depth and the penetration patterns of $LaNO_3$ in the SC were similar; however, the penetration pathways of $LaNO_3$ in the viable epidermis showed different patterns between passive diffusion with a primarily intercellular pathway and combined LFS treatment with TS or OA with a primarily intracellular pathway. This difference in penetration pathway of $LaNO_3$ in the viable epidermis may be explained by a cavitation effect of LFS. LFS is shown to generate cavitation—the formation, oscillation, and collapse of bubbles in an ultrasound pressure field (Rao and Nanda, 2009). The cavitation inside the skin is now thought to be the most important mechanism in LFS-induced skin permeability (Tang

et al., 2002). In the SC, LFS-induced cavitation bubbles interact with SC and generate localized shock waves and liquid microjets directed at the SC surface, resulting in ultrastructural modification of the structure of lipid bilayers in the SC as well as increased lacunae spaces and a theoretical three-dimensional porous network (Tezel and Mitragotri, 2003; Paliwal *et al.*, 2006). In addition, the collapse of cavitation bubbles can generate forced convection in the presence of ultrasound (Morimoto *et al.*, 2005). On the basis of the concept that cavitations are generated as a result of dissolved gases, we expect that in contrast with the SC, which is not a liquid and is too thin to allow large bubbles, the underlying viable epidermis may possess more abundant and well-formed cavities during LFS. The transient collapse of these cavitation bubbles interacting with cells produces high local pressures and temperatures (Frizzell, 1988). This inertial cavitation has been suggested to have a significant role on LFS-mediated membrane permeabilization by two possible mechanisms, including shock waves and shear stresses (Miller *et al.*, 1996; Sundaram *et al.*, 2003). In addition, keratinocytes in the viable epidermis showed a more decreased cell diameter and reduced barrier properties than SC, and therefore the effects of cavitation may influence a broader area (Kushner *et al.*, 2007). From this context, we hypothesized that in the underlying viable epidermis, cavitation effects may increase the membrane permeability of keratinocytes, driving the molecules into both intercellular and intracellular spaces, and resulting in deep penetration.

In this study, we provide morphologic evidence for the synergistic effect of LFS and other penetration enhancers on skin permeability and visualized an ultrastructural pathway of $LaNO_3$ and Fe_3O_4 within the viable epidermal layers. We also visualized the ability of combined treatment of LFS with TS or OA to enhance the penetration of $LaNO_3$ through an intracellular pathway, which supports the morphologic basis for the use of LFS as a method for cellular drug delivery. Finally, it should also be noted that our data obtained with hairless mice skin do not necessarily translate into human skin because the penetration of nanosized molecules may be different among species with different skin architecture and composition. Our results are summarized in Figure 9.

MATERIALS AND METHODS

Animals

Adult hairless mice were purchased from the animal laboratory of Yonsei University and were 8- to 12-week-old females at the time of

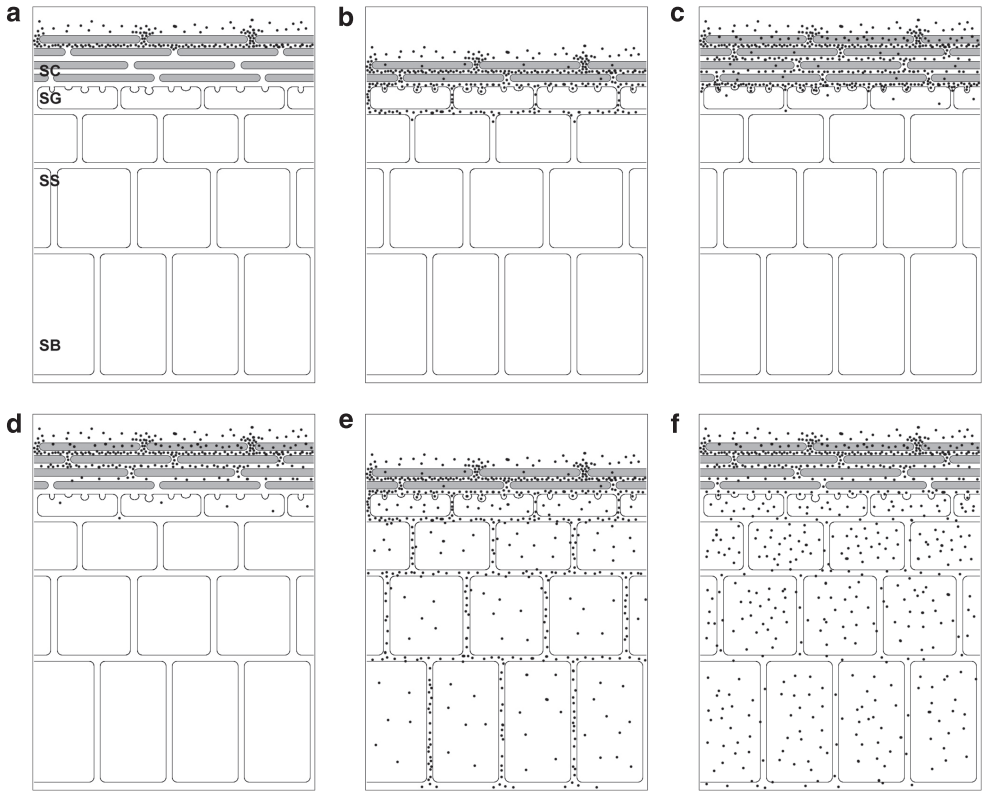

Figure 9. The penetration pathways of $LaNO_3$ after combined treatment of LFS and physical or chemical enhancer. (**a**) When $LaNO_3$ is applied to untreated skin, $LaNO_3$ penetration is restricted to the intercellular spaces in the uppermost SC. (**b**) When $LaNO_3$ is applied to tape-stripped skin or (**c**) OA-treated skin, the penetration is restricted to the SC, SC–SG interface, and occasionally in the upper SG layers with primarily intercellular distribution. (**d**) In LFS-treated skin in the presence of $LaNO_3$, the penetration is extended to the upper SG layer with primarily intercellular distribution. (**e**) In TS/LFS-treated skin or in (**f**) OA/LFS-treated skin, $LaNO_3$ is shown to be uniformly distributed in the full-thickness epidermis (SC–SB layers) with both intracellular and intercellular spaces.

study. The use of mice was approved by the institutional review board of the Yonsei University College of Medicine.

Nanoparticle synthesis and characterization

All synthesis processes of the nanoparticles were carried out in a nitrogen–filled environment by using standard airless techniques. Commercial Iron (II) acetylacetonate, 1,2-hexadecanediol, lauric acid, dodecyl amine, and diphenyl ether, purchased from Aldrich (Milwaukee, WI), were used without further purification. Hydrophobic iron oxide nanoparticles were synthesized through thermal decomposition of $Fe(acac)_3$ (acac = acetylacetonate) in a hot organic solvent by modified procedures previously reported. $Fe(acac)_3$ (2 mmol), 1,2-hexadecanediol (10 mmol), lauric acid (6 mmol), dodecylamine (6 mmol), and diphenyl ether were mixed and magnetically stirred under a flow of nitrogen. A sample of 6 nm Fe_3O_4 nanoparticles dispersed in hexane was added. The mixture was first heated at 150 °C for 30 minutes to remove hexane, and then at 200 °C for 1 hour. Under a blanket of nitrogen, the mixture was further heated to reflux for 30 minutes. The black-colored mixture was cooled to room temperature by removing the heat source. Iron oxide nanoparticles were suspended in hexane at a concentration of 5 mg ml^{-1}. The stock solution (5 mg ml^{-1}) of iron nanoparticles was mixed with 0.3 M oleic acid-stabilizing ligands (1:1 molar ratios of iron oxide to oleic acid) for steric stabilization in nonpolar solutions. The working concentration of the iron nanoparticle was 2.5 mg ml^{-1}. The size and morphology of iron oxide nanoparticles were observed using TEM.

Ultrasound application

Adult female hairless mice were anesthetized with chloral hydrate. Lanthanum nitrate tracer only was applied to the negative control group for 5 minutes. To analyze the penetration pathway of the tracer after LFS, the solution containing lanthanum nitrate tracers was used as a coupling medium. The 3% lanthanum nitrate solution was prepared by dissolving lanthanum nitrate in 0.1 M phosphate buffer. A total of 1% toluidine blue was added to the lanthanum nitrate solution to identify the location of LFS-induced localized transport regions. The working concentration of lanthanum nitrate solution was 1.5% (15 mg ml^{-1}). 50 μl tracer solutions were applied to the backs of hairless mice. The site then immediately received 5 minutes of 800 mW per cm^2, 25-kHz continuous wave ultrasound. The probe was placed directly on the skin surface and the tracer solution was changed every 20 seconds during treatment by turning off the ultrasound. The ultrasonic intensity was measured using an UW-4 ultrasound wattmeter (Fluke Biomedical, Carson City, NV), as described by Tezel *et al.* (2001). Immediately after the exposure period, the tracer solution was removed from the treated area by washing with distilled water and was then dried gently with a cotton swab. After ultrasound application, no visible irritation was observed and blue-colored patches were observed on the skin surface, representing the potential tracer localized transport regions, in which lanthanum nitrates and toluidine blue were concentrated.

In the combined treatment of LFS and physical enhancement, the treatment site was tape stripped and then received LFS treatment with the identical frequency, intensity, and duration. In the combined treatment of LFS and chemical enhancer, OA was dissolved at 0.3 M in distilled water. OA solution was topically applied to the dorsal skin of mice with OA solution-soaked cotton balls for 30 minutes at 5-minute intervals and completely removed from the treated site by distilled water and wiped with a paper towel. The application site then received LFS treatment with the identical frequency, intensity, and duration.

For the visualization and comparison of pathways and the extent of percutaneous penetration of lanthanum nitrates among all treated groups, the same volume and concentration of tracer solutions were applied to each treated site with the same contact time: 50 μl tracer solutions containing 3% lanthanum nitrate were applied every 20 seconds for 5 minutes.

Passive diffusion pathway studies

As the aim of this study was to elucidate the penetration pathway of the tracer across the viable epidermis after combined treatment with LFS and other penetration enhancement methods, it was necessary to perform passive diffusion experiments with an incision technique for delivering tracers across an SC barrier instead of LFS or other penetration enhancement methods as a positive control. A superficial incision was made through the dorsal skin of mice with a sharp scalpel, and 50 μl tracer solutions containing lanthanum nitrates were applied to the site that was breached by scalpel incision.

The second aim of this study was to analyze and compare the transport pathways of two different tracers across the viable epidermis, including lanthanum nitrate and Fe_3O_4 nanoparticle. For purposes of comparison, we applied 50 μl tracer solutions containing Fe_3O_4 nanoparticle to the dorsal skin of mice that were incised with a scalpel in the same way.

Transmission electron microscopy

After treatment, the skin tissues were cut into 1–2 mm^3 pieces and immediately fixed in Karnovsky's fixative for 2 hours at 4 °C. The samples were then washed in 0.1 M phosphate buffer and post-fixed in 1% osmium tetroxide (EMS, Hatfield, PA). For ruthenium tetroxide post-fixation, the specimens were post-fixed in 0.25% ruthenium tetroxide (EMS), 0.1 M phosphate buffer for 45 minutes at room temperature in the dark. Subsequently, the samples were dehydrated in a graded series of ethanol, embedded in a low-viscosity epon–epoxy mixture, and sectioned (UCT, Leica, Germany). Thin sections were unstained and examined under a transmission electron microscope (H-7600, Hitachi, Japan) operating at 80 kV.

Scanning electron microscopy

For scanning electron microscopy, specimens with 0.5–1.0 cm^2 thickness were cut and dried at a critical point drier (HCP-2, Hitachi, Japan) mounted on an aluminum stub. The specimens were then Pt-Pd coated (E-1030, Hitachi, Japan) and examined with a scanning electron microscope (S-4700, Hitachi, Japan).

Penetrated $LaNO_3$ quantification

Penetrated $LaNO_3$ was quantified using image analysis tools (ImageJ, National Institutes of Health). Images were processed by taking fast Fourier transform and/or by convolving images, followed by thresholding to extract tracer spots from the images. The processed images thus obtained only represented tracers, which were then quantified by the ''Analyze Particle'' tool of ImageJ software. The number density and area density of $LaNO_3$ penetrated into the SC layer and the viable epidermal layers were quantified for control, LFS-treated, tape-stripped, OA-treated, TS/LFS-treated, and OA/LFS-treated skin samples.

Statistical analysis

To test the significance of $LaNO_3$ penetration properties on ultrasound treatment, analysis of Student's *t*-test (two-tailed heteroskedastic test) was applied to the data set.

CONFLICT OF INTEREST

The authors state no conflict of interest.

REFERENCES

Baroli B (2009) Penetration of nanoparticles and nanomaterials in the skin: fiction or reality? *J Pharm Sci*; e-pub ahead of print 10 August 2009

Baroli B, Ennas MG, Loffredo F *et al.* (2007) Penetration of metallic nanoparticles in human full-thickness skin. *J Invest Dermatol* 127:1701–12

Bechet D, Couleaud P, Frochot C *et al.* (2008) Nanoparticles as vehicles for delivery of photodynamic therapy agents. *Trends Biotechnol* 26:612–21

Becker BM, Helfrich S, Baker E *et al.* (2005) Ultrasound with topical anesthetic rapidly decreases pain of intravenous cannulation. *Acad Emerg Med* 12:289–95

Degim IT (2005) Understanding skin penetration: computer aided modelling and data interpretation. *Curr Computer-Aided Drug Design* 1:11–9

El-Kamel AH, Al-Fagih IM, Alsarra IA (2008) Effect of sonophoresis and chemical enhancers on testosterone transdermal delivery from solid lipid microparticles: an *in vitro* study. *Curr Drug Deliv* 5:20–6

Elias PM (1983) Epidermal lipids, barrier function, and desquamation. *J Invest Dermatol* 80(Suppl):44s–9s

Frizzell LA (1988) Biologic effects of acoustic cavitation. In: Suslick KS (ed). *Ultrasound, Its Chemical, Physical, and Biologic Effects*. VCH Publisher: New York, 287–303

Gupta AK, Gupta M (2005) Synthesis and surface engineering of iron oxide nanoparticles for biomedical applications. *Biomaterials* 26:3995–4021

Jiang SJ, Zhou XJ (2003) Examination of the mechanism of oleic acid-induced percutaneous penetration enhancement: an ultrastructural study. *Biol Pharm Bull* 26:66–8

Jin S, Ye K (2007) Nanoparticle-mediated drug delivery and gene therapy. *Biotechnol Prog* 23:32–41

Johnson ME, Mitragotri S, Patel A *et al.* (1996) Synergistic effects of chemical enhancers and therapeutic ultrasound on transdermal drug delivery. *J Pharm Sci* 85:670–9

Kierszenbaum AL (2002) *Histology and Cell Biology*. Mosby Inc: St Louis, 305

Kost J, Mitragotri S, Gabbay RA *et al.* (2000) Transdermal monitoring of glucose and other analytes using ultrasound. *Nat Med* 6:347–50

Kushner J IV, Kim D, So PT *et al.* (2007) Dual-channel two-photon microscopy study of transdermal transport in skin treated with low-frequency ultrasound and a chemical enhancer. *J Invest Dermatol* 127:2832–46

Menon GK, Elias PM (1997) Morphologic basis for a pore-pathway in mammalian stratum corneum. *Skin Pharmacol* 10:235–46

Merino G, Kalia YN, Delgado-Charro MB *et al.* (2003) Frequency and thermal effects on the enhancement of transdermal transport by sonophoresis. *J Control Release* 88:85–94

Miller MW, Miller DL, Brayman AA (1996) A review of *in vitro* bioeffects of inertial ultrasonic from a mechanistic perspective. *Ultrasound Med Biol* 22:1131–54

Mitragotri S (2000) Synergistic effect of enhancers for transdermal drug delivery. *Pharm Res* 17:1354–9

Mitragotri S, Kost J (2004) Low-frequency sonophoresis: a review. *Adv Drug Deliv Rev* 27:589–601

Mitragotri S, Ray D, Farrell J *et al.* (2000) Synergistic effect of low-frequency ultrasound and sodium lauryl sulfate on transdermal transport. *J Pharm Sci* 89:892–900

Monti D, Giannelli R, Chetoni P *et al.* (2001) Comparison of the effect of ultrasound and of chemical enhancers on transdermal permeation of caffeine and morphine through hairless mouse skin *in vitro*. *Int J Pharm* 229:131–7

Morimoto Y, Mutoh M, Ueda H *et al.* (2005) Elucidation of the transport pathway in hairless rat skin enhanced by low-frequency sonophoresis based on the solute-water transport relationship and confocal microscopy. *J Control Release* 103:587–97

Naik A, Pechtold LA, Potts RO *et al.* (1995) Mechanism of oleic acid-induced skin penetration enhancement *in vivo* in humans. *J Control Release* 37:299–306

Neuberger T, Schopf B, Hofmann H *et al.* (2005) Superparamagnetic nanoparticles for biomedical applications: possibilities and limitations of a new drug delivery system. *J Magn Magn Mat* 293:483–96

Nohynek GJ, Dufour EK, Roberts MS (2008) Nanotechnology, cosmetics and the skin: is there a health risk? *Skin Pharmacol Physiol* 21:136–49

Ogura M, Paliwal S, Mitragotri S (2008) Low-frequency sonophoresis: current status and future prospects. *Adv Drug Deliv Rev* 60:1218–23

Paliwal S, Menon GK, Mitragotri S (2006) Low-frequency sonophoresis: ultrastructural basis for stratum corneum permeability assessed using quantum dots. *J Invest Dermatol* 126:1095–101

Penn SG, He L, Natan MJ (2003) Nanoparticles for bioanalysis. *Curr Opin Chem Biol* 7:609–15

Prausnitz MR, Langer R (2008) Transdermal drug delivery. *Nat Biotechnol* 26:1261–8

Rao R, Nanda S (2009) Sonophoresis: recent advancements and future trends. *J Pharm Pharmacol* 61:689–705

Rouse JG, Yang J, Ryman-Rasmussen JP *et al.* (2007) Effects of mechanical flexion on the penetration of fullerene amino acid-derivatized peptide nanoparticles through skin. *Nano Lett* 7:155–60

Sundaram J, Mellein BR, Mitragotri S (2003) An experimental and theoretical analysis of ultrasound-induced permeabilization of cell membranes. *Biophys J* 84:3087–101

Tang H, Wang CC, Blankschtein D *et al.* (2002) An investigation of the role of cavitation in low-frequency ultrasound-mediated transdermal drug transport. *Pharm Res* 19:1160–9

Tezel A, Mitragotri S (2003) Interactions of inertial cavitation bubbles with stratum corneum lipid bilayers during low-frequency sonophoresis. *Biophys J* 85:3502–12

Tezel A, Sens A, Mitragotri S (2002) Investigations of the role of cavitation in low-frequency sonophoresis using acoustic spectroscopy. *J Pharm Sci* 91:444–53

Tezel A, Sens A, Mitragotri S (2003) Description of transdermal transport of hydrophilic solutes during low-frequency sonophoresis based on a modified porous pathway model. *J Pharm Sci* 92:381–93

Tezel A, Sens A, Tuchscherer J *et al.* (2001) Frequency dependence of sonophoresis. *Pharm Res* 18:1694–700

Wang MD, Shin DM, Simons JW *et al.* (2007) Nanotechnology for targeted cancer therapy. *Expert Rev Anticancer Ther* 7:833–7